

APPLICATION OF CD-ADAPCO BEST PRACTICES TO NESTOR OMEGA MVG BENCHMARK EXERCISES USING STAR-CCM+

R. Brewster, C. Carpenter, and E. Volpenhein

CD-adapco, 60 Broadhollow Road, Melville, NY 11747, USA

robert.brewster@cd-adapco.com; cassandra.carpenter@cd-adapco.com; eric.volpenhein@cd-adapco.com

E. Baglietto

Department of Nuclear Science and Engineering, Massachusetts Institute of Technology,

77 Massachusetts Avenue, Cambridge, MA 02139, USA

emiliob@mit.edu

J. Smith

Toyota Racing Development, 1125 Competition Dr., Salisbury, NC 28146

jeff_smith@toyota.com

ABSTRACT

Computational Fluid Dynamics (CFD) is being applied to assess the propensity for adverse localized conditions affecting nuclear reactor fuel performance, including crud-induced-localized-corrosion (CILC), grid-to-rod-fretting, and departure from nucleate boiling, with unprecedented precision. In keeping with advances in computer resources, such analyses have evolved from isolated analysis of local behavior, e. g., a single coolant channel, to highly resolved integral analysis of representative fuel bundles and beyond.

The Electric Power Research Institute (EPRI) recently organized a NESTOR CFD Round Robin benchmark project to quantify the effectiveness of CFD in discerning local variations in fuel cladding temperature in prototypic PWR fuel bundles, primarily for the purposes of CILC assessment. The benchmark additionally evaluated and assimilated best practices contributed by participants for industry awareness.

STAR-CCM+, a commercial CFD-based modeling & simulation environment broadly used in the nuclear power industry, was prominently featured in the NESTOR Benchmark by numerous participants. This paper more specifically details modeling and analysis of the NESTOR heated-bundle mixing vane grid test (OMEGA MVG) by CD-adapco, developers of STAR-CCM+. Implementation of CD-adapco best practices is described to properly discretize the geometry, assign physical models and boundary conditions, faithfully represent material properties, and specify efficient solution controls in a manner that respects the numerical methods employed. Results for the OMEGA MVG blind benchmark case are also analyzed in additional detail. The techniques presented herein are demonstrated to produce exceptional results with commonly available computational resources and have been contributed to the NESTOR CFD Benchmark report for industry awareness.

Keywords: PWR fuel performance, CFD Benchmark, CILC, Mixing vane grid, NESTOR

1.0 INTRODUCTION

Over the past several years, industry initiatives in pursuit of zero fuel failures have increased attention on axial and azimuthal variation in fuel cladding and reactor coolant temperatures during normal operation as

an important factor in Crud-Induced-Power-Shifts (CIPS) and Crud-Induced-Localized-Corrosion (CILC). Under certain circumstances, a highly resolved analysis of local conditions is advised to augment conventional core design and management practices [1]. Computational fluid dynamics (CFD) is being applied to this effect [2, 3]. In keeping with advances in computer resources, such analyses have evolved from single-phase analysis of selected coolant channels and grid spans, to integral analysis of whole fuel bundles and beyond. An expanding body of work also explores the influence of boiling and two phase flow.

Attention has likewise been given to both proprietary and collaborative benchmarks to assess and improve CFD for this purpose [4-8]. Among the challenges in such benchmarks is measurement of local conditions and recording of experimental setup with sufficient resolution and detail to enable comparison with CFD results in a fundamentally revealing manner. Highly resolved modeling of fuel bundles at prototypic scale can also formidably challenge the capacity of current CFD technology. Nevertheless, a common finding is that CFD, when properly applied, uniquely advances the understanding of complex fluid flow and heat transfer phenomena within rod bundles in a practical manner. To that end, deliberate application of specific methods and techniques within the context of CFD, a. k. a, best practices, and acute awareness of their limitations are additionally highlighted as inseparable from interpretation of results. However, conclusions regarding the suitability of CFD and associated best practices, particularly for quantitative analyses, are generally left to the analyst with knowledge of the specific circumstance and purpose intended.

Accordingly, to assist industry in the specific purpose of Level IV CIPS and CILC assessment in PWR cores in accordance with [1], EPRI convened a NESTOR [9] CFD Benchmark project in 2009. Participants in the NESTOR CFD Benchmark, which included fuel suppliers, software developers, universities, a research organization, and a utility, volunteered to model a selection of tests from the NESTOR experimental program for comparison with measured data. A primary objective of the NESTOR CFD Benchmark, which recently concluded, was to gain and report insights into generally applicable best practices for predicting local cladding and coolant temperatures in PWR fuel bundles under prototypic, single phase operating conditions. An additional objective was to establish a measure of reliability one could expect in results as they pertain to CIPS and CILC assessment.

The NESTOR experimental program produced high quality and highly resolved thermal-hydraulic data on 5×5 rod bundles in prototypic PWR conditions. From a CFD modeling perspective, the test bundles also featured a challenging pattern of alternating simple support grids (SSG) and mixing vane grids (MVG) representative of operating plants. Both isothermal (MANIVEL) and heated (OMEGA) test bundles were investigated. The former provided pressure loss data and local axial velocity measurements via LDV. The latter contributed highly resolved cladding temperature data and discrete coolant temperatures at subchannel centers. A particularly distinctive contribution of the heated bundle tests was high quality, circumferentially resolved cladding temperatures at various axial locations within the heated length.

The work and findings of the NESTOR CFD Benchmark, which encompass a collection of open and blind benchmark exercises spanning different fuel bundle configurations and operating conditions are compiled in [10] and described in a conference special session of NURETH 16 [11]. STAR-CCM+, a commercial CFD-based modeling & simulation environment broadly used in the nuclear power industry, featured prominently in the work. This paper augments the benchmark report with details of the STAR-CCM+ modeling and analysis of the NESTOR heated mixing vane grid test (OMEGA MVG) by CD-adapco, developers of STAR-CCM+. The OMEGA MVG test is viewed by CD-adapco as most challenging for the CFD modeling process because of the geometric scale, intricate detail of the mixing vane grids, high swirl flow, and multi-dimensional conjugate heat transfer.

2.0 OMEGA MVG TEST OVERVIEW

Details of the NESTOR experimental setup and test conditions are reported in [9 – 11] and selected elements are summarized here for clarity and convenience. For purposes of this paper, the specific setup of interest is the heated mixing-vane-grid bundle, known as OMEGA MVG.

The central feature of the OMEGA MVG test is a vertically oriented 5 x 5 square array of heated Inconel 600™ tubes with uniform outer tube diameter (9.5mm) and pitch (12.6mm). An insulated square casing encloses the bundle with a uniform 3.1 mm rod-to-wall gap enforced between the perimeter tubes and the casing. The total length of tubes is approximately 5m with a heated length of 3.658m. A schematic of the OMEGA MVG test bundle and tube array is reproduced from [9] and [10] as Figure 2-1.

The tubes are secured within the casing by a sequence of support grids alternating between a simple support grid design and a MVG design representative of the commercial Westinghouse 17×17 V5H design. The MVGs are additionally installed in two alternating orientations, MVG O1 and MVG O2, with MVG O2 rotated 90° clockwise with respect to MVG O1. The positions of the support grids in the instrumented section are shown in Figure 2-1.

Although all tubes have the same outer diameter, the cladding of the 9 inner tubes (0.90 ± 0.1 mm) is thicker than the cladding of the 16 perimeter tubes (0.675 ± 0.1 mm). The 9 inner tubes are also equipped with an interior thermocouple probe that can be repositioned axially over the uppermost 1.2m of heat length and rotated along the inner tube surface to measure temperature at selected points. The thermocouple probes are designed to provide good thermal contact and as precise as possible point contact with the tube inner-surface. The contact sensing area reportedly increased over the course of the NESTOR tests due to wear, but maintained a circumferential contact angle of less than 15° nonetheless.

Three pressurized steady-state test series were included in the NESTOR CFD Benchmark for the OMEGA MVG. In each case, flow was delivered at a uniform, constant rate and temperature beneath the test bundle some distance beneath the lowest support grid and was directed upward through the bundle.

Voltage was applied through the heated length of the tube bundle generating a virtually uniform and constant volumetric heat source within the tube cladding via joule heating. Power generated in each of the inner tubes was proportionately greater than in each of the perimeter tubes because of the thicker cladding.

For each test series, detailed 2-dimensional distributions of tube inner-surface temperatures were obtained over the four uppermost grid spans within the nine central tubes. The NESTOR CFD Benchmark more specifically compared modeling results with data from three tubes (Rod 1, Rod 2, and Rod 5 in Figure 2-1b) at 8 axial locations ranging from 1150 mm to 850 mm below End of Heated Length (EOHL). Coolant temperatures over the bundle cross-section were also obtained at the EOHL by point measurement reportedly within ± 1.5 mm of the center of the subchannels.

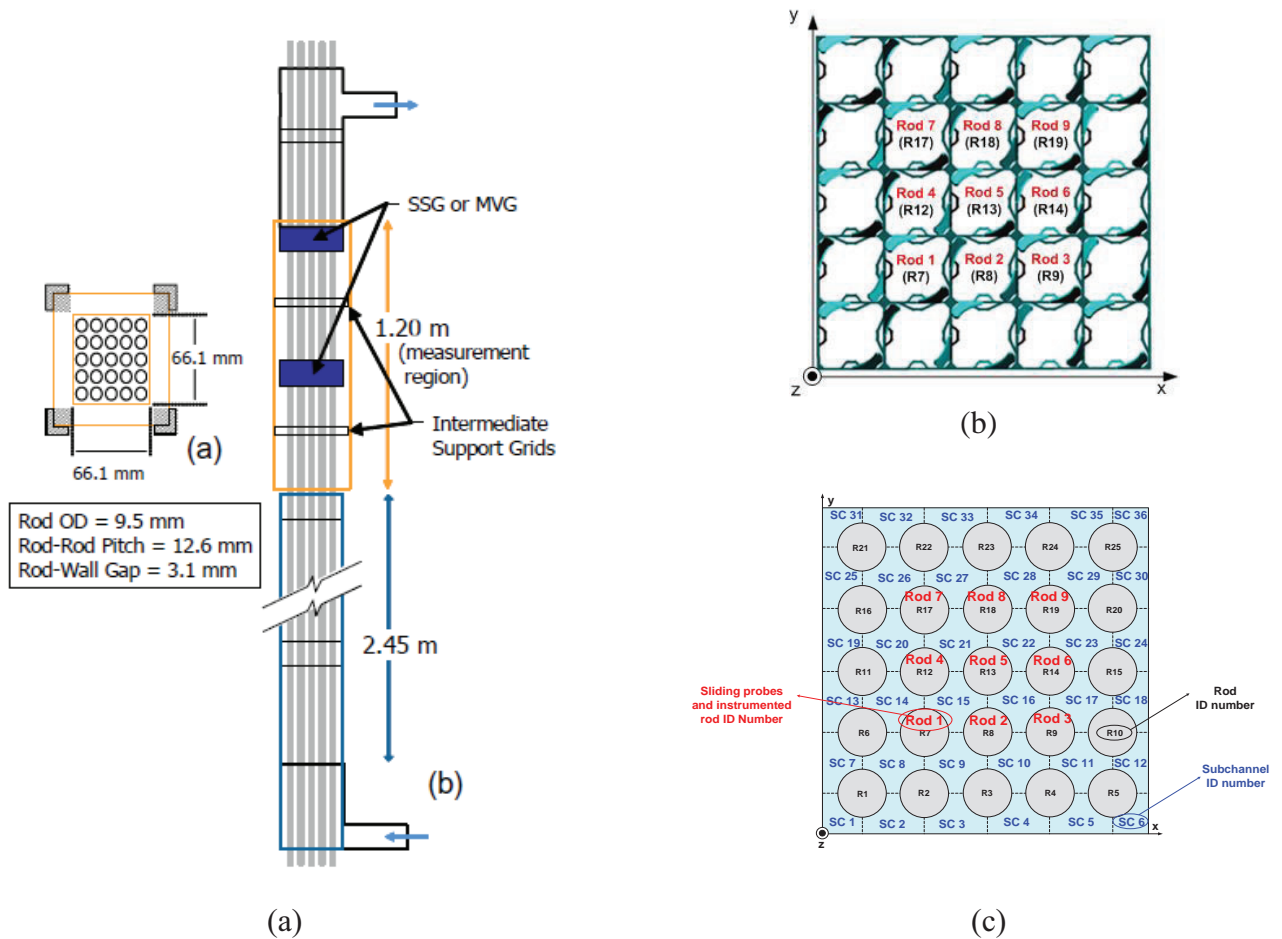


Figure 2-1. OMEGA MVG (a) Test Bundle Schematic, Reproduced from [9], and (b) MVG O2 Orientation and (c) Tube Array, Reproduced from [10]

3.0 STAR-CCM+ MODEL SETUP

CFD modeling in its most complete sense and as applied to the NESTOR CFD Benchmark is a multi-faceted, interconnected process generally recognized to include some fashion of geometry definition, discretization (a. k. a., mesh generation), specification of pertinent physics models, assignment of boundary conditions and material properties, and numerical solution and post-processing / reporting. STAR-CCM+ offers a distinctly integrated and complete capability to execute the process in an efficient and reliable manner. A wealth of techniques are enabled to meet the needs of virtually any circumstance and available compute resource. Those applied to the NESTOR CFD Benchmark were informed by many years of successful application to diverse nuclear fuel designs and are described in the following sections.

3.1 Computer Resources

A model encompassing the full tube bundle cross section and heated length with explicit representation of the spacer grid boundaries was considered to assess compute resource needs. This enabled the cumulative effects of the added heat and the complex pattern of mixing vanes to be incorporated in the most versatile and efficient manner. Sufficient discretization of the tube cladding was also necessary to resolve local

variations in cladding temperature arising from non-uniform conjugate heat transfer and joule heating. Accordingly, available memory for meshing, solution, and data processing was a primary consideration in the selection of compute resources and in the model development.

A 256 Gb workstation with contemporary GPU graphics processing was committed to the NESTOR CFD Benchmark. A resource of this capacity can generally be expected to accommodate a STAR-CCM+ hex-dominated, trimmed-cell finite volume model incorporating several hundred million cells. In contrast, the single phase, steady-state RANS solution presented a relatively modest, scalable computational load. Analyses were run on a 10 node system having 16 cores per node and equipped with high band-width interconnect. Runtimes less than 2 days were typical.

3.2 Geometry Preparation

The modeling process in STAR-CCM+ began by defining the fluid and solid domains from geometric data. To this end, a 3D CAD model of the grid spacer designs were provided to all benchmark participants in three file formats: Parasolid, STEP and IGES. Dimensional data previously described was supplied directly for tubes, assembly casing, measurement locations, etc. A fluid domain corresponding to a section of tube bundle co-located with a grid spacer was first created for each of the spacer designs. These were used in modular fashion for construction of the complete model as follows.

The CAD data in Parasolids format was initially imported directly into a session of STAR-CCM+ and retained as a single tessellated surface for each grid design. To produce a suitable modeling domain and high-quality computational mesh, the surfaces described therein were examined to ensure they were closed, non-manifold, and non-self-intersecting. STAR-CCM+ provides capabilities for inspecting, locally modifying (e.g. filling holes, collapsing and zipping edges), and tessellating the CAD data, if needed, to accomplish this. However, the imported CAD data for the MVG and SSG grid spacer designs were clean and closed, so the use of these surface repair techniques was not required.

Following standard practice, grid spacer elements designed to contact the tube surfaces were also closely inspected to identify tangential points of contact or gaps that might otherwise result in unnecessary and problematic mesh refinement. The 3D CAD module within STAR-CCM+ enables integrated CAD capabilities to mitigate such circumstances. These capabilities include sketch-based solid body creation through extrusion, revolution, slicing and lofting operations. Modification of existing solid bodies is also possible via cutting and Boolean operations to unite, subtract or intersect solid bodies. Other utilities include hole-filling as well as de-featuring operations such as filleting and blending. In the case of the NESTOR CFD Benchmark, tangential points of contact were extruded a small amount into the adjacent cladding surface and trimmed via Boolean subtraction to create a discernable contact area.

The 3D CAD capability of STAR-CCM+ was used to generate bodies representing the 9 central and 16 peripheral tubes. This was accomplished by creating a 2D sketch of a 25-rod square array, using the specified tube outer diameter and pitch provided as part of the benchmark specification. The rod cross sections were initially constructed using a 720 point spline to accommodate reported manufacturing variability in the outer diameter of the rod. However, this effect was later shown to be insignificant in course of the NESTOR CFD Benchmark and a simple circular sketch was used for the work presented here. The rod array sketch was then extruded in the axial direction to create a body representative of the total length of the 25 rods.

Next, one MVG O1, one MVG O2, and one SSG grid were each centered in their own a rectangular box with cross-sectional dimensions of the bundle casing. These were extruded axially 10mm below and above each grid. Using a multi-object Boolean subtraction, the volume occupied by the grid and 25 tubes was then removed from each box. The remaining portion formed a fluid domain for each grid type. These were

then replicated and repositioned axially to create the grid segments of the fluid domain for the complete test section (Figure 2-1a).

The upstream and downstream faces of each grid fluid segment were delineated by feature angle and assigned as periodic boundaries with the downstream face of one segment paired with the upstream face of the next segment in sequence. During mesh generation in STAR-CCM+, this enforces a conformal discretization on the boundaries to the fullest extent possible. The full length fluid domain was lastly derived during meshing through a straightforward, stepwise extrusion process described in Section 3.3 to manage memory demands.

Finally, the full length cladding geometry was extruded during the meshing process beginning with a 2D sketch of the tube array in a similar manner as the rods array. In the case of the tube array, however, the center portions corresponding to the tube inner diameters were first removed from the sketch prior to extrusion to create the proper cladding geometry.

3.3 Mesh Generation

STAR-CCM+ incorporates a versatile, highly automated meshing process to create unstructured, form-fitted finite volume meshes of fluid and solid domains. Mesh generation is automatically informed by the surface tessellation and CAD elements that define the geometry, such as local curvature, surface proximity, and retained feature elements, and is further controlled by user-specified meshing parameters. The latter are organized into a hierarchy of global specifications and local refinements that enables precise control to achieve cell quality metrics, such as skewness, connectivity, conformity, near-wall cell properties, and growth rate with the smallest practical mesh even for exceptionally intricate geometries. STAR-CCM+ also employs a face-based solver technology uniquely designed to recognize arbitrary polyhedral cell topology.

Specific meshing selections used for the OMEGA MVG test geometry followed CD-adapco best practices for tube bundles, which are optimized considering a variety of factors common to such applications. Among them is the dominant axial flow direction over most of the tube bundle length, a circumstance for which the use of a hex-dominated, trimmed cell mesh offers greater meshing efficiency. A base size of 0.3 mm was assigned for the fluid domain subject to automatic local refinement to resolve geometric details within the constraints of a 0.075 mm minimum mesh dimension and growth factor less than 1.3. A standard wall function and compatible turbulence model is also specified to model stress in the viscous sublayer and laminar-to-turbulent transition region, with turbulent advection represented via Reynolds Analogy. Hence, the trimmed-cell inflation process in STAR-CCM+ was set to establish a layer of prismatic cells maintaining a y^+ value in the near-wall cell within the target range between 30 and 150 to the fullest extent practical. A single prismatic near wall layer of 0.15 mm for the bare rod segments accomplished this.

In portions of the bundle occupied by spacer grids, especially MVG designs, momentum imparted by the grids tends to influence fluid flow and heat transfer throughout the bundle to a much greater extent than local heat transfer in the grid segment. Thus, in the OMEGA MVG model, prejudice was given to resolving the relevant geometric features of the grids. Accordingly, feature retention, curvature, proximity refinement, and growth rate were limiting factors for mesh sizing in these fluid segments. The y^+ wall function constraint was sacrificed where necessary at these locations.

To create the full length fluid volume, the periodic boundaries of the MVG and SSG grid segments were extruded during the meshing process to meet mid-span, thus creating a set of meshed fluid segments each extending upstream from mid-span to the mid-point of the downstream span. This allowed for axial stretching to be incorporated in the regions between the grid spacer segments with an aspect ratio of 5

achieved. Since in STAR-CCM+ the periodic specification essentially enforces a conformal discretization on the paired boundaries, the extruded mesh segments were also virtually conformal. These were then merged in STAR-CCM+ to construct a monolithic mesh for the full length fluid volume.

For the tube mesh, a small axial section of the 25 tube array was extruded from a 2D sketch and meshed using STARCCM+'s thin mesh feature. The thin mesh feature creates a specified number of polyhedral elements with predominantly hex-based cross sections between two surfaces. For the OMEGA MVG model, 6 layers were used between the tube inner and outer diameters. The mesh boundary was then extruded in similar fashion to the fluid domain to form an axially uniform hex mesh of the entire length of the tube array and the initial section was removed. The tube mesh was then aligned and interfaced with the mesh of the full length fluid domain using an indirect mapped interface. Figure 3-1 shows cross sections of the mesh from (a) the tube bundle region, (b) a MVG segment, and (c) an SSG segment. The full length mesh consisted of 284 million finite volume cells including fluid volume and cladding.

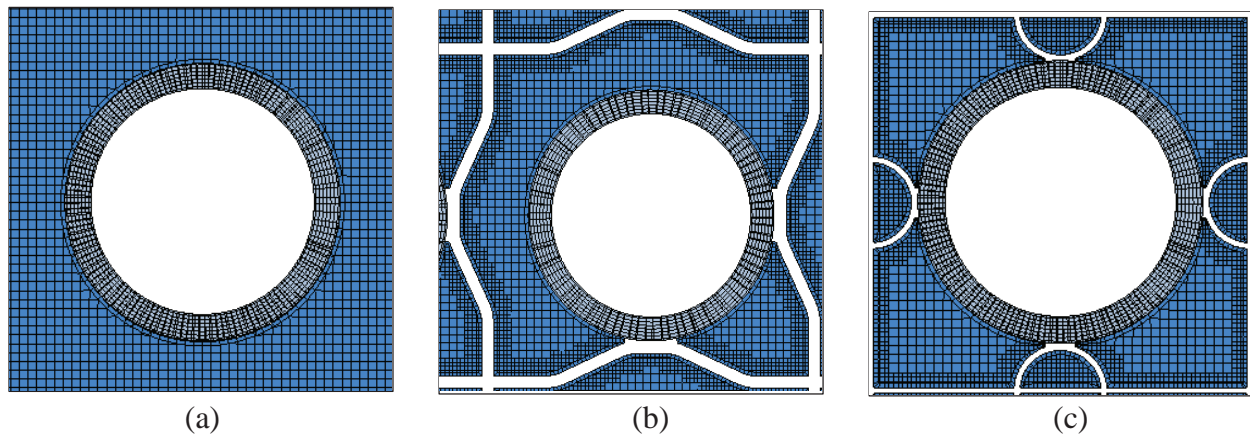


Figure 3-1 View of Mesh through (a) Tube Bundle (b) MVG Segment and (c) SSG Segment

3.4 Analysis Specifications

Steady-RANS calculations were performed adopting a segregated flow solver based on the SIMPLE algorithm for Pressure-Velocity coupling, and applied on collocated variables with Rhie-Chow interpolation [12, 13]. All convective terms were approximated with a non-oscillatory upwind based 2nd order scheme, using the Venkatakrishnan reconstruction gradient limiting. In accordance with CD-adapco best practices, a high y^+ implementation of a non-linear quadratic K-Epsilon turbulence model [14] with standard wall function was selected; the model allows including in the simulation the essential effect of flow anisotropy.

The heat generation was incorporated through a constant volumetric heat source for each central tube and each perimeter tube as appropriate. Temperature-dependent properties for the cladding as provided with benchmark specifications were interpolated from a table. The fluid was modeled as incompressible water with a turbulent Prandtl number of 0.9 and temperature-dependent density and specific heat specified via a polynomial. Dynamic viscosity was interpolated from a table.

A uniform mass flux inlet and inlet temperature were assigned to match experimental conditions. A uniform static pressure outlet was specified somewhat beyond the EOHL. The tube enclosure and grid spacer

boundaries were represented as a smooth, adiabatic, no-slip surface. Conjugate heat transfer was permitted from the outer tube walls, which were also defined as smooth and no slip. The inner tube walls were modeled as adiabatic.

In addition to solver residuals, volume-averaged temperature, surfaced averaged temperature, mass balance, and pressure differentials in various segments were monitored to confirm convergence.

4.0 RESULTS

Results from CD-adapco were submitted to the NESTOR CFD Benchmark organizer in accordance with specifications. The specifications were appropriately designed to facilitate the collective comparison with measured data and results from other participants. When analyzed within the context of the full NESTOR CFD Benchmark program, which also includes findings from LDV and pressure loss data from the isothermal hydraulic tests (MANIVEL series), reduction in this manner revealed insights into the suitability and limitations of specific models and methods. The following discussion complements the NESTOR CFD Benchmark report [10-11] by examining the results with focus on the use of CFD to predict trends in local cladding temperature and heat transfer in synergistic fashion with less resolved analysis methods, e. g., subchannel codes. It also supplements the work of the NESTOR CFD Benchmark by exploring the influences of thermocouple contact area and EOHL probe locations on the comparison between data and CFD results.

To this end, Figure 4-1 presents the calculated tangential velocities across the tube bundle at three different axial locations, beginning 30 mm downstream from the top of the first MVG in the measurement section and two other locations before the next MVG. The non-uniform distribution with well-defined, coherent vortex structures near the center of flow channels characteristic of vane-type grid spacers is clearly evident near the MVG. These structures become progressively eccentric and less distinct downstream. Tangential flows and coherent flow structures are virtually unnoticeable 460 mm downstream after passing the mid-span SSG and approaching the next MVG.

Also presented in Figure 4-1 are corresponding local fluid temperatures relative to the cross-sectional average fluid temperature ($T - T_{avg}$). The distribution of near-wall fluid temperatures is observed to strongly correlate with that of the tangential velocities, i. e., high temperature coincides with low tangential velocity near the cladding and vice versa. Exceptions emerge around the outer tubes due to the proximity of the unheated enclosure. These become more apparent downstream as the magnitudes of local tangential velocities generally diminish and integral effects on bulk coolant temperature become commensurately more influential. Although not shown here for brevity, in this analysis the near-wall fluid temperature is an effective surrogate with respect to this correlation for the distribution of local cladding temperature.

For quantitative assessment, the circumferential variations in inner clad temperature around a central tube (Rod 5) are shown in Figure 4-2 for various axial locations between MVGs, also beginning 30 mm downstream of the first MVG of instrumented section. At that elevation, the temperatures are observed to vary -6 to +8 °K relative to the average temperature in a developing sinusoidal fashion with a period of 180°. A more uniform sinusoidal distribution is present at 230 mm downstream of the MVG with lower amplitude ranging from -4 to 5.3°K. A review of the more complete results indicate that amplitudes peak at just over +8 °K 70 mm downstream before reaching less than $\pm 2^\circ\text{K}$ near the next MVG segment. A transition in the distribution is apparent as the bi-polar influence of the MVG vanes on local heat transfer diminishes and the quadrupole influence of the square rod array re-emerges.

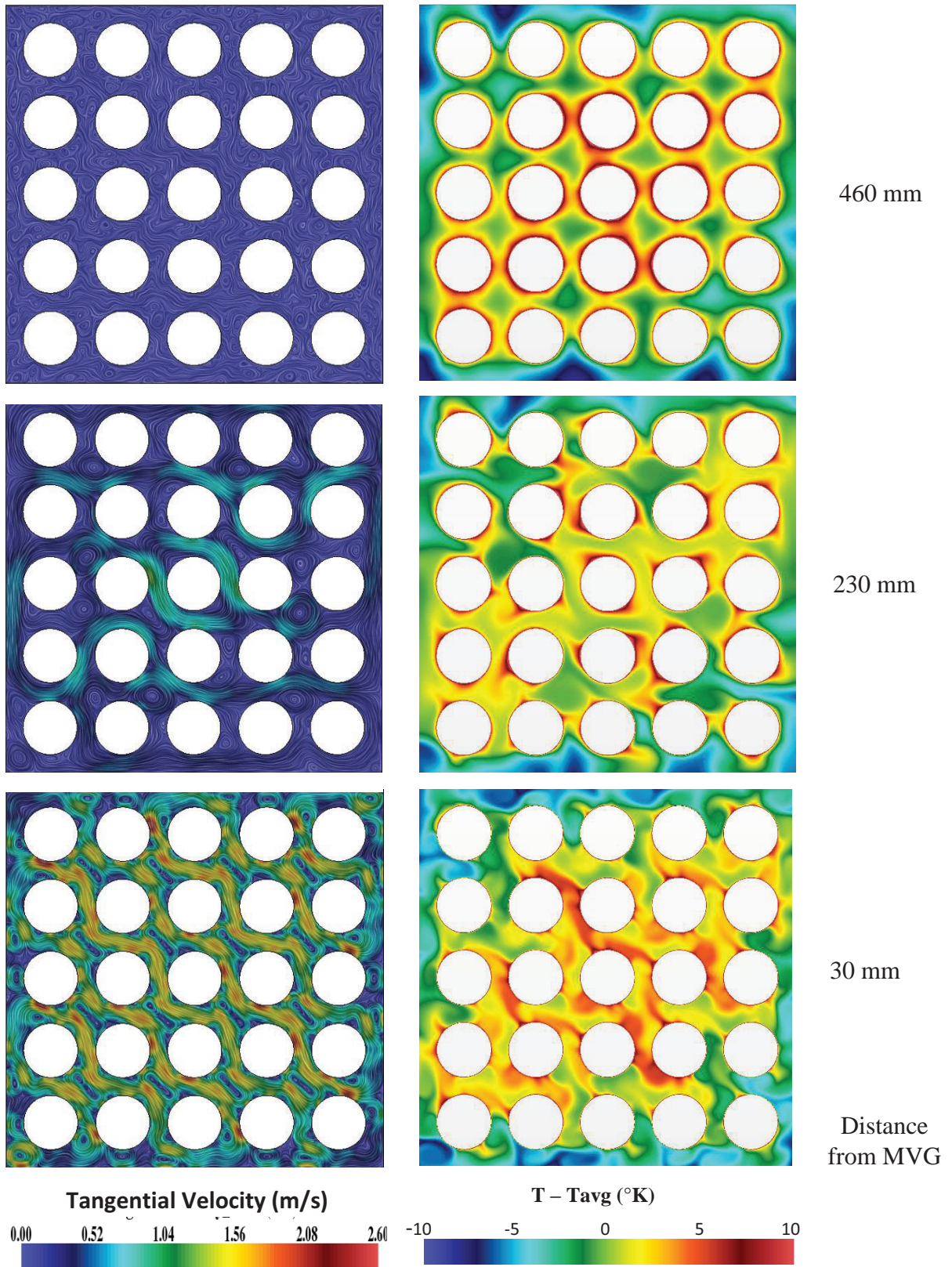


Figure 4-1: Tangential Velocities and Fluid Temperatures Downstream of MVG

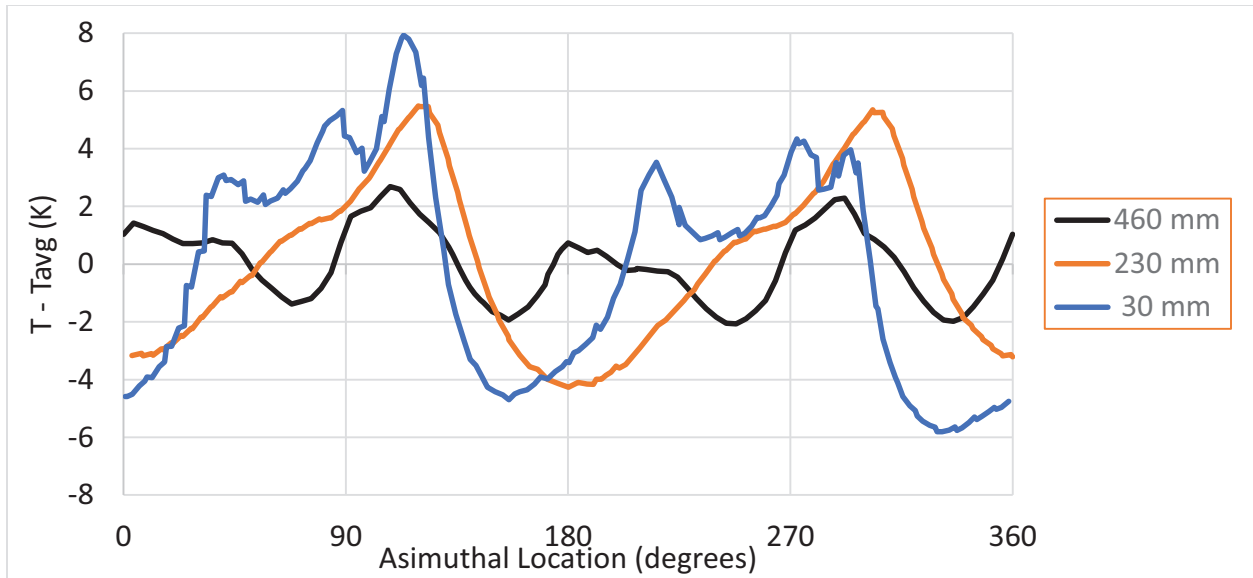


Figure 4-2: Circumferential Variation in Rod 5 Inner Wall Temperature with Distance from MVG

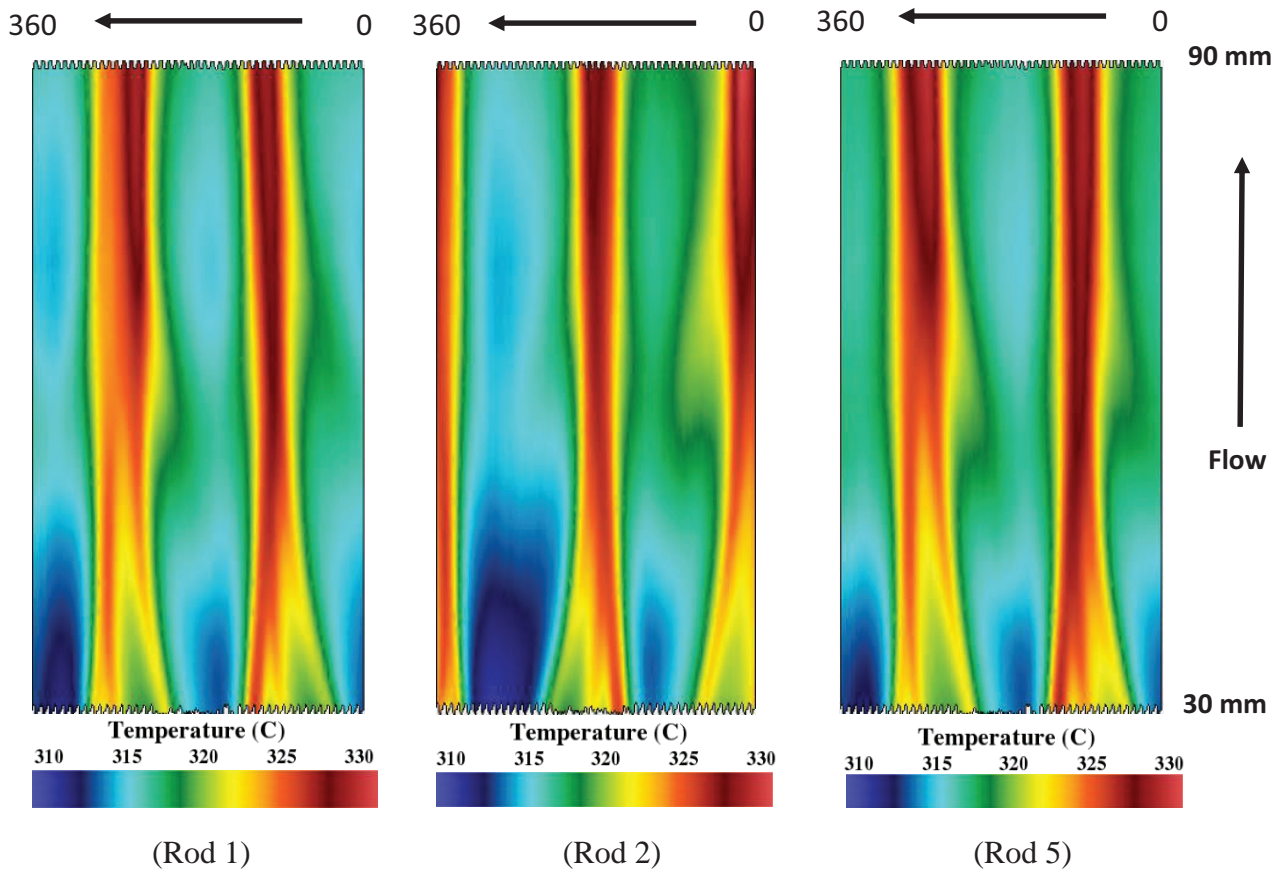


Figure 4-3 Inner Wall Cladding Temperatures for Rods 1, 2, and 5 from 30 mm to 90 mm Downstream of the MVG at 1108 mm before EOHL

Trends in cladding temperature are also revealed using the projection technique demonstrated in Figure 4-3, which compares inner wall temperature results for Rods 1, 2, and 5 displayed as unfolded tube segments. Patterns of streaks highlight the azimuthal variations in outer wall temperatures with axial distance. The streaks are observed to develop over approximately the first 70 mm from the mixing vane and remain relatively persistent for some distance thereafter.

The distribution in local heat transfer coefficient (HTC) relative to that calculated based on subchannel average conditions was also computed from the CFD results using 30 mm elevation of Rod 5 as a representative location. For this analysis, the bulk fluid temperature was calculated as the axial-mass-flux-weighted average of local fluid temperatures within the adjacent subchannel (see Figure 2-1c). The local heat flux and outer wall temperature were used directly. Results are presented in Figure 4-4. The local HTC was observed to vary approximately -20% to +38% about the mean HTC for the corresponding subchannel quadrant.

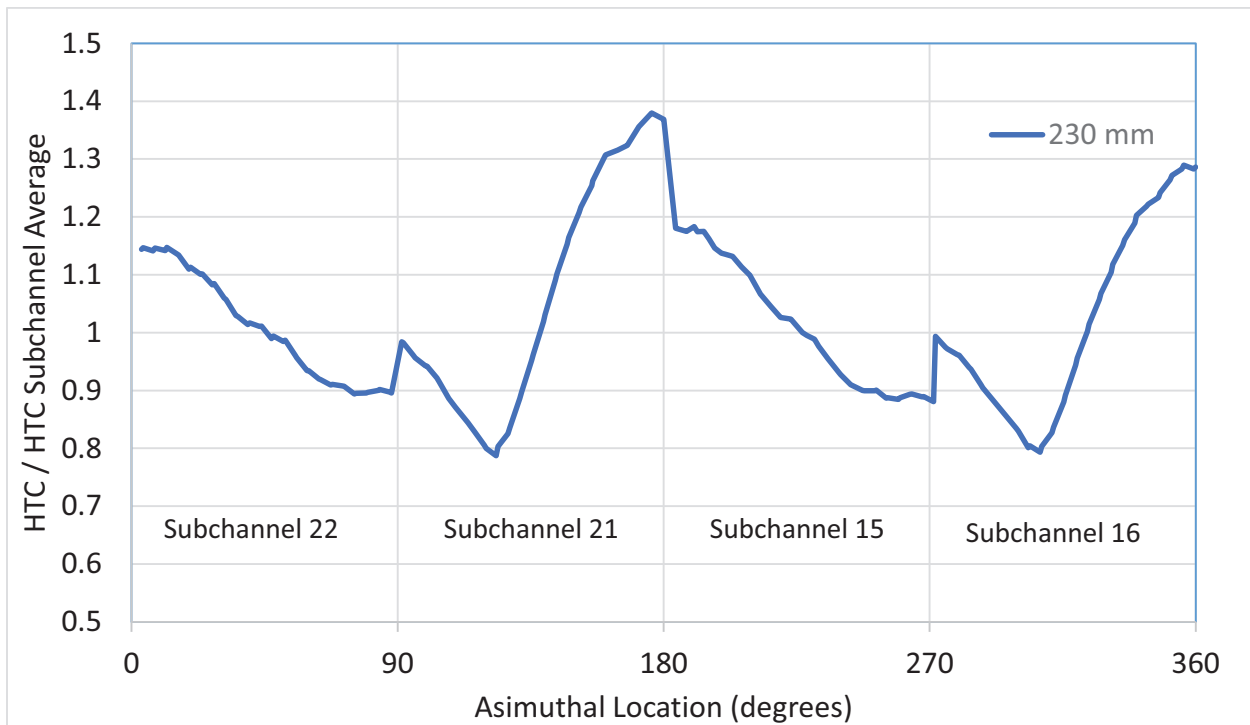


Figure 4-4 Variation of Local Heat Transfer Coefficient for Rod 5 at Elevation -879 mm Relative to Subchannel Average

The NESTOR CFD Benchmark also suggested contact area of the thermocouple probe as a potential influence in differences between the measured cladding temperature and CFD results. The latter were broadly reported to overestimate the measured peak temperature. Uncertainty in EOHL probe location was also noted as a possible influence in comparison with calculated results for notably different trends were reported in some subchannels. The STAR-CCM+ results were further explored in this work to compare the distribution of local cladding temperatures for the 30 mm elevation with those averaged over

an arc length of $15^\circ (\pm 7.5^\circ)$ about each location. This is reported as an upper bound on the contact area for the thermocouple. The arc-averaged temperature is found to decrease the peak variation by no more than 0.25°K at this axial location.

The sensitivities of reported EOHL subchannel center temperatures to probe location were also investigated. For the OMEGA MVG setup, the thermocouple probes were noted to be placed within ± 1.5 mm of the design center. Results from STAR-CCM+ were interrogated for a sampling of subchannels to determine the variation in calculated fluid temperature this distance from the centers. The EOHL temperatures were found to vary $+2^\circ\text{K}$ to -1.4°K over this distance.

5.0 CONCLUSIONS

Computational Fluid Dynamics, as demonstrated through the use of STAR-CCM+, has developed into a practical technology for examining multi-dimensional single phase fluid flow and heat transfer in PWR fuel assemblies at prototypic scale and operating conditions. For purposes of maintaining long term fuel reliability, the technology is generally capable of resolving azimuthal variations in local cladding temperature throughout the fuel assembly arising from conjugate heat transfer to the coolant. Furthermore, the influence of contemporary design elements, such as mixing vane grids, is also discernable and quantifiable. When used in combination with findings from the NESTOR CFD Benchmark or other validation exercises, CFD is a reliable engineering tool to complement standard design practices when additional details about local conditions is beneficial. This work additionally highlights the synergy between CFD and experimental setup & procedures, with the former providing a means to estimate the precision of the latter on the measured data and vice versa.

ACKNOWLEDGEMENTS

The authors wish to acknowledge EPRI, EdF, and CEA for their contribution of the NESTOR experimental details and, together with Texas A & M University, their efforts to organize and facilitate the NESTOR CFD Benchmark. The collaboration of all the participants and the support of CD-adapco enabling our participation are also gratefully acknowledged. The assistance and critique of CD-adapco application engineer, Sampat Nidadavolu, in careful generation and confirmation of the final images and other details of this paper are especially appreciated.

REFERENCES

- [1] *Fuel Reliability Guidelines: PWR Fuel Cladding Corrosion and Crud, Revision 1, Volume 1*, EPRI, Palo Alto, CA, Product 3002002795, 2014
- [2] J. Jones, M. Martin, T. Keheley, R. Harne, M. Pop, C. Lascar, J. Simoneau, AREVA's Comparative Process for CILC Risk Assessment Using Subchannel and CFD Modeling, *ICONE20-POWER2012-54552*, 2012
- [3] Ling Zou, Hongbin Zhang, Jess Gehin and Brendan Kochunas, A Coupled TH/Neutronics/CRUD Framework in Prediction of CIPS Phenomenon, *Nuclear Technology 2012*
- [4] B. Neykov, F. Aydogan, L. Hochreiter, K. Ivanov, H. Utsuno, F. Kasahara, E. Sartori, M. Martin, NUPEC BWR Full-size Fine-mesh Bundle Test (BFBT) Benchmark, Volume I: Specifications," *NEA/NSC/DOC(2005)5*, 2006
- [5] A. Rubin, A. Schoedel, M. Avramova, H. Utsuno, S. Bajorek, and A. Velazquez-Lozada, OECD/NRC Benchmark Based on NUPEC PWR Subchannel and Bundle tests (PSBT), Volume I: Experimental Database and Final Problem Specifications, *NES/NSC/DOC(2010)1*, 2010.

- [6] A. Tentner, S. Lo, D. Pointer, A. Splawski, Advances in the Development and Validation of CFD-BWR, a Two Phase Computational Fluid Dynamics Model for the Simulation of Flow and Heat Transfer in Boiling Water Reactors, *Proceedings of the 14th International Conference on Nuclear Energy*, 2006
- [7] S. Lo, J. Osman, CFD Modeling of Boiling Flow in PSBT 5×5 Bundle, *Science and Technology of Nuclear Installations*, 10.1155/2012/795935, 2012
- [8] M. Conner, E. Baglietto, A. Elmahdi, CFD Methodology and Validation for Single-Phase Flow in PWR Fuel Assemblies, *Nuclear Engineering and Design*, 2010
- [9] A. Bergeron, T. Chataing, E. Décossin, J. Garnier, P. Péturaud, S. K. Yagnik, Design, Feasibility, and Testing of Instrumented Rod Bundles to Improve Heat Transfer Knowledge in PWR Fuel Assemblies, *Proceedings of the International LWR Fuel Performance*, 2007
- [10] *Computational Fluid Dynamics Benchmark of High Fidelity Fuel Rod Bundle Experiments – Industry Round Robin Phase 2 – Mixing Vane Grids*, EPRI, Palo Alto, CA, 2015
- [11] D. Wells, P. Peturaud, S. K. Yagnik, Overview of CFD Round Robin Benchmark of the High Fidelity Fuel Rod Bundle NESTOR Experimental Data, *Proceedings of the 16th Nuclear Reactor Thermal Hydraulics Conference*, Chicago, IL, 2015
- [12] J. Ferziger, M. Peric, Computational Methods for Fluid Dynamics, *Springer-Verlag*, 1999.
- [13] C. Rhie, W. Chow, Numerical study of the turbulent flow past an airfoil with trailing edge separation, *AIAA Journal* 21 (1983) 1525–1532.
- [14] E. Baglietto, Anisotropic Turbulence Modeling for Accurate Rod Bundle Simulations, *Proceedings of 14th International Conference on Nuclear Energy*, 2006